Monthly Notices of the ROYAL ASTRONOMICAL SOCIETY

MNRAS **513,** 3482–3492 (2022) https://doi.org/10.1093/mnras/stac1002
Advance Access publication 2022 April 13

Serendipitous discovery of radio flaring behaviour from a nearby M dwarf with MeerKAT

Alex Andersson [1]★ Rob P. Fender [1,2] Chris J. Lintott [1] David R. A. Williams [3] Laura N. Driessen [3,4] Patrick A. Woudt [2] Alexander J. van der Horst [5,6] David A. H. Buckley [2,7,8] Sara E. Motta [9] Lauren Rhodes [1,10] Nora L. Eisner [1] Rachel A. Osten [11,12] Paul Vreeswijk,[13] Steven Bloemen [13] and Paul J. Groot [2,7,13]

[1]*Astrophysics, Department of Physics, University of Oxford, Denys Wilkinson Building, Keble Road, Oxford OX1 3RH, UK*
[2]*Department of Astronomy, University of Cape Town, Private Bag X3, Rondebosch 7701, South Africa*
[3]*Jodrell Bank Centre for Astrophysics, Department of Physics and Astronomy, The University of Manchester, Manchester M13 9PL, UK*
[4]*CSIRO, Space and Astronomy, PO Box 1130, Bentley, WA 6102, Australia*
[5]*Department of Physics, The George Washington University, 725 21st Street NW, Washington, DC 20052, USA*
[6]*Astronomy, Physics and Statistics Institute of Sciences (APSIS), 725 21st Street NW, Washington, DC 20052, USA*
[7]*South African Astronomical Observatory, PO Box 9, Observatory 7935, South Africa*
[8]*Department of Physics, University of the Free State, PO Box 339, Bloemfontein 9300, South Africa*
[9]*Istituto Nazionale di Astrofisica, Osservatorio Astronomico di Brera, via E. Bianchi 46, I-23807 Merate (LC), Italy*
[10]*Max-Planck-Institut für Radioastronomie, Auf dem Hügel 69, D-53121 Bonn, Germany*
[11]*Space Telescope Science Institute, 3700 San Martin Drive, Baltimore, MD 21218, USA*
[12]*Center for Astrophysical Sciences, Johns Hopkins University, Baltimore, MD 21218, USA*
[13]*Department of Astrophysics/IMAPP, Radboud University, PO 9010, NL-6500 GL Nijmegen, the Netherlands*

Accepted 2022 April 4. Received 2022 March 11; in original form 2021 December 6

ABSTRACT

We report on the detection of MKT J174641.0−321404, a new radio transient found in untargeted searches of wide-field MeerKAT radio images centred on the black hole X-ray binary H1743−322. MKT J174641.0−321404 is highly variable at 1.3 GHz and was detected three times during 11 observations of the field in late 2018, reaching a maximum flux density of 590 ± 60 μJy. We associate this radio transient with a high proper motion, M dwarf star SCR 1746−3214 12 pc away from the Sun. Multiwavelength observations of this M dwarf indicate flaring activity across the electromagnetic spectrum, consistent with emission expected from dMe stars, and providing upper limits on quiescent brightness in both the radio and X-ray regimes. *TESS* photometry reveals a rotational period for SCR 1746−3214 of 0.2292 ± 0.0025 d, which at its estimated radius makes the star a rapid rotator, comparable to other low-mass systems. Dedicated spectroscopic follow up confirms the star as a mid-late spectral M dwarf with clear magnetic activity indicated by strong Hα emission. This transient's serendipitous discovery by MeerKAT, along with multiwavelength characterization, make it a prime demonstration of both the capabilities of the current generation of radio interferometers and the value of simultaneous observations by optical facilities such as MeerLICHT. Our results build upon the literature of M dwarfs' flaring behaviour, particularly relevant to the habitability of their planetary systems.

Key words: stars: activity – stars: flare – stars: late-type – radio continuum: stars – radio continuum: transients.

1 INTRODUCTION

Radio telescopes have, until recently, been primarily of use for variable and transient searches as follow-up instruments, typically informed by detections at higher energies such as optically transient supernovae, gamma-ray bursts (GRBs), and X-ray binaries (XRBs). However, with the advent of the current generation of wide field radio interferometers, including Square Kilometre Array (SKA) pathfinder instruments like MeerKAT (Camilo et al. 2018), the Australian SKA Pathfinder (ASKAP; Johnston et al. 2007), the Murchison Widefield Array (MWA; Tingay et al. 2012), and the LOw Frequency ARray (LOFAR; Van Haarlem et al. 2013), the astronomical community can now sample the radio sky with improved sensitivity and, crucially, with larger fields of view (FoVs).

To date, the number of serendipitously detected, image plane radio transients remains low. This is in contrast to the well-established coherent population of variable radio sources such as pulsars and fast radio bursts (see Fender & Bell 2011; Pietka, Fender & Keane 2015, for a discussion on coherent and incoherent transients) that are discovered regularly in untargeted searches. Ongoing image plane searches for radio transients include the ASKAP survey for Variables and Slow Trasients (VAST; Murphy et al. 2013) and the Amsterdam–ASTRON Radio Transients Facility and Analysis Centre (AART-

★ E-mail: alexander.andersson@physics.ox.ac.uk

© The Author(s) 2022.
Published by Oxford University Press on behalf of Royal Astronomical Society. This is an Open Access article distributed under the terms of the Creative Commons Attribution License (http://creativecommons.org/licenses/by/4.0/), which permits unrestricted reuse, distribution, and reproduction in any medium, provided the original work is properly cited.

Downloaded from https://academic.oup.com/mnras/article/513/3/3482/6567874 by Deutsches Elektronen Synchrotron DESY user on 05 June 2022

FAAC; Prasad et al. 2016), along with large field surveys such as the Karl G. Jansky Very Large Array's (VLA) Sky Survey (VLASS; Lacy et al. 2020). A number of transients have been discovered at frequencies ranging from tens of MHz to a few GHz for which there have yet to be associated multiwavelength counterparts or definite progenitor systems (e.g. Hyman et al. 2005; Bower et al. 2007; Ofek et al. 2011; Jaeger et al. 2012; Stewart et al. 2016; Murphy et al. 2017; Varghese et al. 2019; Wang et al. 2021). Large surveys have shown that, in the radio band, many variable and transient phenomena can be attributed to scintillation or intrinsic AGN variation (e.g. Levinson et al. 2002; Bannister et al. 2011; Mooley et al. 2016; Bhandari et al. 2018; Radcliffe et al. 2019; Driessen et al. 2022). For example, Sarbadhicary et al. (2021) utilize the VLA's COSMOS HI Legacy Survey to create a Variable and Explosive Radio Dynamic Evolution Survey (CHILES VERDES), which makes use of the plethora of multiwavelength data of the COSMOS field and 5.5 yr worth of data reaching RMS sensitivities of $\sim$10 μJy beam^{-1} per epoch. Their results reach low flux density limits and find 58 AGN-type sources using the moderate FoV of radius 22.5 arcmin. From this literature, only $\sim$1–5 per cent of the radio sky seems to be variable, with the number of confirmed Galactic sources limited primarily to follow-up or targeted observations of known variables. Mooley et al. (2016) associate two of their transients with known types of active star whilst Driessen et al. (2020) describe the first commensally discovered image plane transient from MeerKAT, MKT J170456.2−482100, similarly associating it with a known stellar system. One of the common conclusions arrived at by much of the radio variability literature is that, in order to systematically find radio transients, high sensitivity, regular cadence and large FoVs are required and that surveys lacking any of these three pillars can limit detection capabilities.

ThunderKAT[1] (Fender et al. 2016) is the MeerKAT Large Survey Project (LSP) dedicated to image plane radio transients. This project uses MeerKAT's 64 dishes and FoV $>$ 1 square degree to take regular cadence observations of reported transients such as XRBs, cataclysmic variables, and GRBs, whilst also operating commensal searches of internal and cross-LSP data. ThunderKAT also makes use of the robotic optical facility MeerLICHT (65 cm primary mirror; Bloemen et al. 2016) that was built and is operated to support transient work with MeerKAT. MeerLICHT observes simultaneously with night-time MeerKAT observations, allowing for better characterization of the multiwavelength transient sky. Both dedicated and commensal work from the ThunderKAT team is bearing fruit and herein we follow in the footsteps of Driessen et al. (2020) by reporting on the discovery of MKT J174641.0−321404, the second serendipitous, image plane radio transient found by MeerKAT, and associate it with a known, nearby red dwarf.

Radio transients have been seen originating from some late-type dwarf stars, typically as a result of magnetic activity and reconnection. These systems are sometimes referred to as 'dMe' stars due to the near ubiquitous presence of hydrogen emission lines, indicative of chromospheric heating (Cram & Mullan 1979; Cram & Giampapa 1987); for reviews of stellar radio astronomy across the Hertzsprung–Russell diagram and on dwarf flares see Güdel (2002) and Osten (2007) respectively. Some of the pioneers of radio astronomy observed radio flares from late-type dwarfs, including the prototypical class namesake UV Ceti (Lovell, Whipple & Solomon 1963; Lovell 1969). Stellar radio flares are caused by either incoherent cyclotron or gyrosynchrotron emission of electrons caught in magnetic fields, or coherent bursts attributed to either plasma- or electron cyclotron maser-emission, which probe the local electron density and magnetic field strength, respectively. For a detailed review of the emission processes in radio bright stars, we refer the reader to Dulk (1985). Most radio observations of flare stars have focused on a few nearby sources such as UV Ceti, Proxima Centauri, AD Leonis, and YZ Canis Minoris (Lacy, Moffett & Evans 1976; Bastian 1990; Slee, Willes & Robinson 2003; Villadsen & Hallinan 2019), however, Pritchard et al. (2021) utilized the circular polarization capabilities of ASKAP to detect coherent emission from 23 stars with no previous radio counterparts. This was done with data reaching an rms sensitivity of 250 μJy beam^{-1} across the entire sky south of $+41^\circ$ declination, again emphasizing the need for wide-field observations. ASKAP has also been used to detect elliptically polarized radio pulses from UV Ceti (Zic et al. 2019). In just the past year, Driessen et al. (2021) have found radio emission coming from the previously known X-ray flare star EXO 040830-7134.7 – a chromospherically active M-dwarf of spectral type M0V – and Callingham et al. (2021) detailed the detection of coherent emission from 19 M dwarfs with LOFAR.

In Section 2, we detail the radio observations and source discovery, whilst Section 3 reconciles said observations with archival optical and X-ray data. Section 4 presents dedicated spectroscopy before the discussion and conclusions of Sections 5 and 6, respectively.

2 RADIO OBSERVATIONS

As part of the ThunderKAT monitoring program, XRB H1743−322 was observed at weekly cadence for 11 epochs, following reports of new outburst behaviour (Williams et al. 2020). Weekly monitoring of this field ran from 9th September until the 10th of November 2018, with each observation consisting of 15 minutes on source and an integration time of 8 seconds. The on source observations were preceded and succeeded by 2 minutes on the phase calibration source J1712−281 or J1830−3602, whilst the band-pass calibrator PKS J1939−6342 was observed for 10 minutes before beginning each observation block. These observations were taken using the *L*-band (900–1670 MHz) receiver, with a central frequency of 1284 MHz, bandwidth of 856 MHz and 4096 frequency channels. The data were reduced using the standard procedure, from flagging with AOFLAGGER (Offringa, Van De Gronde & Roerdink 2012) and calibration using CASA (Mcmullin et al. 2007) through to imaging with WSCLEAN (Offringa et al. 2014; Offringa & Smirnov 2017). For full details on the data reduction, see Williams et al. (2020).

2.1 TraP

The MeerKAT images were run through the LOFAR Transients Pipeline (TRAP; Swinbank et al. 2015) to detect serendipitous varying and transient sources in the large FoV observations. This pipeline does source finding and association across all epochs and constructs a data base of sources and their associated light curves. From each source's light curve, variability statistics η and V are calculated. The former, defined for N flux density measurements $I \pm \sigma$ of weighted mean ξ, as

$$\eta = \frac{1}{N-1} \sum_{i=1}^{N} \frac{(I_i - \xi_{I_N})^2}{\sigma_i^2} \quad (1)$$

describes their reduced chi-squared value when compared to a stable source i.e. constant flux density sources are expected to have $\eta \approx 1$ whilst variable sources produce values greater than unity. V

[1]The HUNt for Dynamic and Explosive Radio transients with MeerKAT.

Downloaded from https://academic.oup.com/mnras/article/513/3/3482/6567874 by Deutsches Elektronen Synchrotron DESY user on 05 June 2022

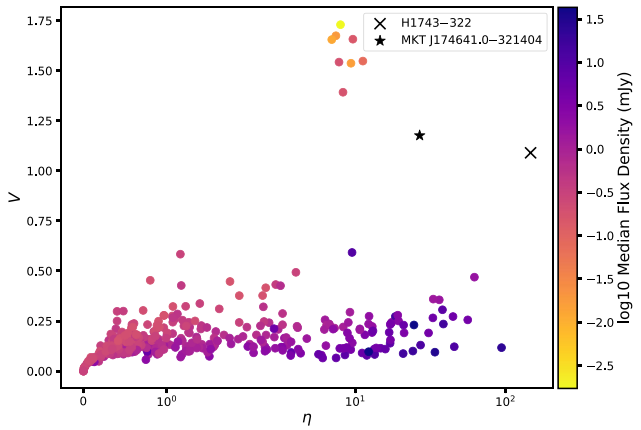

Figure 1. Variability parameters for all sources detected in the H1743−322 field during ThunderKAT observations in late 2018. Clear outliers, particularly in V can be seen, including the XRB H1743−322 itself, several manually vetted artefacts, and an unknown source.

is sometimes known as the modulation parameter or co-efficient of variability and is the ratio of the sample standard deviation to the mean of its flux measurements. In general, sources with large values for both V and η are likely to be identified as transients or variable. For more information on how TRAP processes data and calculates its statistics refer to Swinbank et al. (2015) or other studies using the pipeline (e.g. Rowlinson et al. 2019, Driessen et al. 2020 or Sarbadhicary et al. 2021).

The TRAP was first run with default parameters, analysing the H1743−322 field out to approximately 1.5× the primary beam radius (∼45 arcmin). During fitting, each source is assumed to be the size of the synthesized beam as here we are only interested in the unresolved point source variability. Using the default 8σ detection threshold above the local noise, 377 individual sources were detected across all epochs. This threshold was used as a trade-off between being inundated with many false positives and missing genuine transients. The resultant TRAP variability parameter distributions are detailed in Fig. 1, showing outliers to typical η and V parameters (i.e. $V \gtrsim 0.75$ and $\eta \gtrsim 100$). We note that ∼50 per cent of sources lie below $\eta = 1$, whilst those above are either bright sources with very little variability (η is approximately proportional to signal-to-noise ratio squared), or extended sources whose variation is artificially caused by the shape of the synthesized beam changing between epochs. The grouping of high-V sources were all inspected by eye and found to be imaging or processing artefacts near bright sources. Two highly significant astrophysical sources were identified. One, reassuringly, was the target of this field, the candidate black hole XRB H1743−322, and the other was MKT J174641.0−321404, a hitherto unknown radio source located ∼5≈ arcmin East of the aforementioned XRB.

This previously unknown radio source was detected serendipitously twice during the final four epochs of observation, at a maximum of 590 ± 60 μJy and can be seen to appear and disappear in the radio images of Fig. 2. Running TRAP whilst monitoring the source's location during every time-step allows us to better understand the emission from MKT J174641.0−321404 and provide better constraints on its variability. The resulting light curve from such forced photometry of the source over all epochs can be seen in Fig. 3's upper panel, where non-detections (defined as flux measurements detected at <3σ above local noise) are indicated with faint points. The source can be seen to be detected during the first epoch of observation, at ∼3.5σ. Fig. 3's lower panel shows marginal evidence for intra-epoch variability, wherein the brightest detection of MKT J174641.0−321404 has been split into 5–3-min integrations. At ∼5 arcmin removed from the phase-centre of the radio images, the flux calibrations for this source are imperfect. However, the true values will not be so dissimilar as to invalidate our findings, especially as we are primarily interested in relative variations, and so no further observations have been made nor primary beam corrections applied to correct the light-curve values.

3 ARCHIVAL MULTIWAVELENGTH ASSOCIATION

The radio position of the source is taken to be the weighted mean of the three detection epochs using the Python Blob Detector and Source Finder (PYBDSF; Mohan & Rafferty 2015), differing slightly from TRAP as the former includes the first epoch's detection. At the time of research, cross-matching this mean position of $17^{\rm h}46^{\rm m}41\overset{\rm s}{.}0$, $-32^\circ14'04''(266\overset{\circ}{.}6709, -32\overset{\circ}{.}2343)$ with the SIMBAD data base[2] returns two objects within 2 arcmin, the optical sources SCR 1746−3214 (henceforth SCR 1746, detection detailed in Boyd et al. 2011) and *Gaia* DR2 4055567846152508160. The latter is ∼97 arcsec from the radio emission and so is likely too distant to be the origin thereof. SCR 1746 has an ICRS J2000 position of $17^{\rm h}46^{\rm m}40\overset{\rm s}{.}659 - 32^\circ14'04\overset{''}{.}50$ with uncertainties of 0.10 and 0.8 mas, respectively, calculated from *Gaia* data release 2 (Gaia Collaboration 2016, 2018), placing it at an on-sky distance from the radio coordinates of 4.″5. SCR 1746 has a *Gaia*-calculated distance from the Sun of $12.06^{+0.1}_{-0.2}$ pc (Bailer-Jones et al. 2018). Taking into account this star's high proper motion μ of $(205.4 \pm 0.2, 103.0 \pm 0.1)$ mas yr^{-1} in Right Ascension and Declination, respectively, this star is 1.″3 from the radio source. This is within the 2σ positional uncertainty of the radio position where $\sigma = 1\overset{''}{.}2$ and so we associate the radio transient events of MKT J174641.0−321404 as originating from SCR 1746. The next nearest optical source in the q-band MeerLICHT image (see below and Fig. 4) is >20 arcsec away.

Multiwavelength coverage from MeerLICHT (Bloemen et al. 2016) confirms this association. A stack of q-band (440–720 nm) exposures taken on 2019 July 7th, July 9th, and 16th and 2020 July 28th form the MeerLICHT reference image for this field, where the small temporal gap between the radio and optical observations renders proper motion effects negligible. The region surrounding MKT J174641.0−321404 can be seen in Fig. 4, showing the proper motion of the *Gaia* source to within positional uncertainties of both the MeerKAT and MeerLICHT objects. This confirms that the radio transient coincides with SCR 1746. We note that there are no observations simultaneous with the radio data as the strict MeerKAT-MeerLICHT coupling was not fully in-place during 2018, early in the life of the projects. In contemporary observations, MeerLICHT follows MeerKAT pointings when possible, though the opposite is not true, hence there being no ThunderKAT data taken during MeerLICHT observations.

3.1 Optical and near-IR photometry

There is substantial photometric sky survey coverage of SCR 1746. Catalogued measurements of this source include the Two-Micron

[2]Set of Identifications, Measurements, and Bibliographies for Astronomical Data, accessed via http://simbad.u-strasbg.fr/simbad/. At time of first research in spring 2021, only SCR 1746−3214 was returned when cross-matching at this search radius.

Downloaded from https://academic.oup.com/mnras/article/513/3/3482/6567874 by Deutsches Elektronen Synchrotron DESY user on 05 June 2022

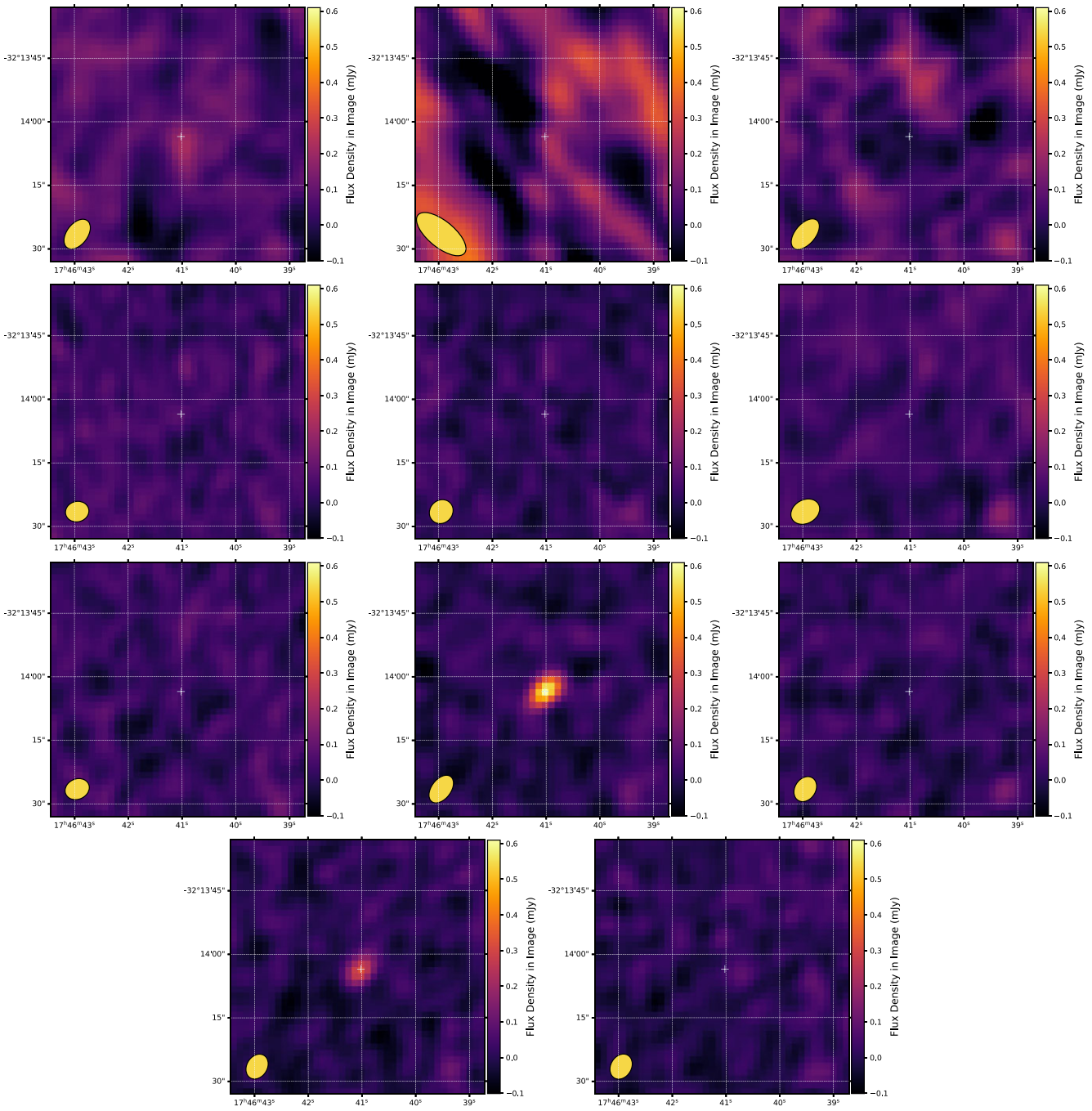

Figure 2. 1 arcmin square images of MKT J174641.0−321404 and surrounding noise during all ThunderKAT observations, running chronologically from top left, across then down. The source can be clearly seen to appear and disappear multiple times across all epochs. The synthesized beam of each image can be seen in the bottom left of each panel, whilst the white central cross-hairs show the source's mean MeerKAT position.

All-Sky Survey (2MASS; Cutri et al. 2003; Skrutskie et al. 2006), the AllWISE data release (Cutri et al. 2013), US Naval Observatory B catalog (USNO-B; Monet et al. 2003), GLIMPSE Source Catalog (Spitzer Science Center 2009), and the optical SuperCOSMOS-RECONS (SCR) southern sky proper motion searches (Boyd et al. 2011). A non-exhaustive summary of some of the recorded magnitudes of this source can be found in Table 1 and is intended to illustrate the source's photometric properties of being relatively bright and red.

SCR 1746 (Tess Input Candidate 111898820; Stassun et al. 2019) was also observed by NASA's Transiting Exoplanet Survey Satellite (*TESS*; Ricker et al. 2015) during Sector 39 of the extended mission. The data, which span 27.9 d between 2021 May 27 and June 24 June, consist of observations obtained every 2 s. These images were combined into 2-min cadence data products onboard of the spacecraft prior to being processed and reduced by the Science Processing Operations Center (SPOC; Jenkins et al. 2016). The full *TESS* data set, shown in Fig. 5 binned to 2-min and 30-min cadence,[3] shows

Downloaded from https://academic.oup.com/mnras/article/513/3/3482/6567874 by Deutsches Elektronen Synchrotron DESY user on 05 June 2022

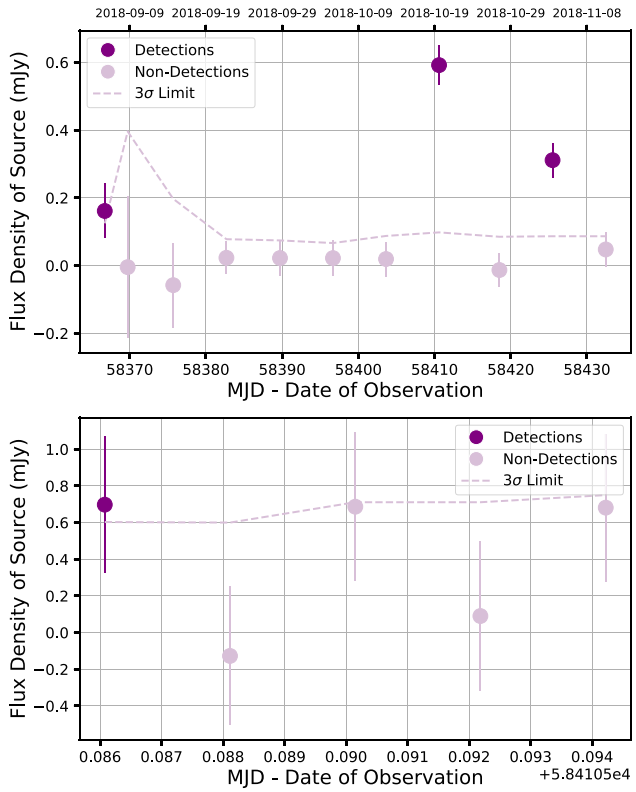

Figure 3. *Upper:* Radio light curve of MKT J174641.0−321404 across all 11 ThunderKAT observation epochs. Non-detections are defined as measurements below a 3σ threshold (dashed line), where σ is the local rms noise in that epoch. The non-physical measurements in some epochs are caused by the forced photometry and epoch-specific noise structure, visible in Fig. 2. The higher detection threshold (due to more noise) in the first three epochs is likely due to the use of a different phase calibrator than the later observations. *Lower:* Radio light curve compiled from 5 × 3 min slices of the brightest 15 min epoch. From this we can see evidence for marginal variability within the epoch.

clear flares that reach up to 30 times quiescent brightness levels. The data were searched using a Lomb–Scargle periodogram (Lomb 1976; Scargle 1982) to identify periodic signals in the light curve, revealing a significant periodicity with a period of 0.2292 ± 0.0025 d. When phase folding the *TESS* light curve at this period, a sinusoidal fit to the data produces a best-fitting relative amplitude of 0.52 ± 0.01 (bottom panel of Fig. 6). There are some background sources on the same *TESS* pixel, but at *G* magnitudes of 18.9 or fainter (cf. 13.95 for SCR 1746) we conclude that these are all too faint to be causing the observed modulation. As can be seen in the top panel of Fig. 6, more flares tend to occur between phase 0 and 0.5, corresponding to the brightest parts of the phase curve. This is in keeping with the photometric modulation being caused by magnetically active spots and associated bright plages rotating into or out of view. If we assume that the star rotates as a rigid body with radius R (see Section 3.1.1) we can express the photometric period as a tangential velocity $v_t = 2\pi R/P = 32.2 \pm 0.9$ km s^{-1}, demonstrating that SCR 1746 is a fast rotator, comparable to other low-mass systems (cf. Gizis et al. 2017 for other dwarfs, or the solar value of ∼2 km s^{-1}).

[3]We note that the chosen binning matches the *TESS* Full Frame Image timescale by coincidence.

Additional optical monitoring of the source is provided by both MeerLICHT (see Section 1) and the All-Sky Automated Survey for Supernovae (ASAS-SN, a global network of 24 40-cm telescopes; Shappee et al. 2014; Kochanek et al. 2017). The optical data in Fig. 7 span almost 4 yr of observations in Johnson's *V*, Sloan *ugriz*, and *q*-band filters. MeerLICHT rotates between filters every 2 min, allowing for quasi-simultaneous colour determination (see Section 3.1.1). From the MeerLICHT data, we can clearly see the star is much brighter at redder wavelengths. Aperture photometry at a 5σ detection threshold from the ASAS-SN Sky Patrol portal shows that optical flares are likely to have been observed from this source in the *g* band. Despite this, none of the optical or radio flares are simultaneous to within <0.4 d. Given that flares can be as short as minutes, this is not unexpected behaviour. Similarly, the photometric period observed by *TESS* is not observed in these data due to infrequent sampling with diurnal and seasonal gaps.

3.1.1 Photometric spectral typing

The latest version of the *TESS* Input Catalog (TIC v8; Stassun et al. 2019) estimates the target to have an effective temperature of 2870 ± 160 K, a mass of 0.12 ± 0.02 $M_\odot$, and radius of 0.146 ± 0.004 $R_\odot$. Sebastian et al. (2021) compile a target list of ultracool dwarf systems in preparation for *TESS*, wherein an empirical relationship for $T_{\rm eff}(M_{\rm H})$ from Filippazzo et al. (2015) is inverted to show that the target has a spectral type of M5.1. Their calculated temperature, mass, and radius are all slightly different than, but consistent with, those from Stassun et al. (2019). The effective temperature scale of M dwarfs given by Rajpurohit et al. (2013) also indicates that a temperature of ∼2900 K is in agreement with a mid-M spectral typing. Finally, MeerLICHT observations provide quasi-simultaneous colours $(r - i) = 2.22 \pm 0.02$ and $(i - z) = 1.09 \pm 0.02$, in agreement with typical values for M6 stars (West, Walkowicz & Hawley 2005; Douglas et al. 2014).

3.2 X-ray observation and correlation

X-ray counts from the 7 yr *Swift*-XRT point source catalogue (1SWXRT; D'Elia et al. 2013), taken over a total exposure time of 4631.1 s on the H1743−322 field are found to be coincident within positional uncertainties of SCR 1746. Assuming an absorbed power-law spectrum, the associated X-ray source has a 0.3–10 keV flux upper limit of 1.68 × 10^{-13} mW m^{-2}, measured at $S/N = 2.8$. 1SWXRT has been superseded by the *Swift*-XRT Point Source catalogs 1 and 2 (1SXPS; Evans et al. 2014, 2SXPS; Evans et al. 2020), both of which contain nearby sources (separation in 1SXPS = 7″.5, 2SXPS = 2″.31), but that do not formally lie close enough to the *Gaia* position for association within a 90 per cent confidence interval region. As such, herein we use the analysis from 1SWXRT, but it is worth noting that the equivalent fluxes for the nearest sources in 1SXPS and 2SXPS, respectively, are ∼1.16× and ∼0.43× the 1SWXRT flux, so the overall conclusions made here would still broadly apply.

There is a known relation between the quiescent radio ($L_{\rm R}$) and X-ray ($L_{\rm X}$) luminosities of several types of active star, indicating a connection between the non-thermal, energetic electrons causing the radio emission and the bulk coronal plasma responsible for thermal X-rays:

$$\log(L_X) \lesssim \log(L_R) + 15.5 \quad (2)$$

(Guedel & Benz 1993; Benz & Guedel 1994). The standard interpretation of this Güdel and Benz relation is that magnetic reconnection in

Downloaded from https://academic.oup.com/mnras/article/513/3/3482/6567874 by Deutsches Elektronen Synchrotron DESY user on 05 June 2022

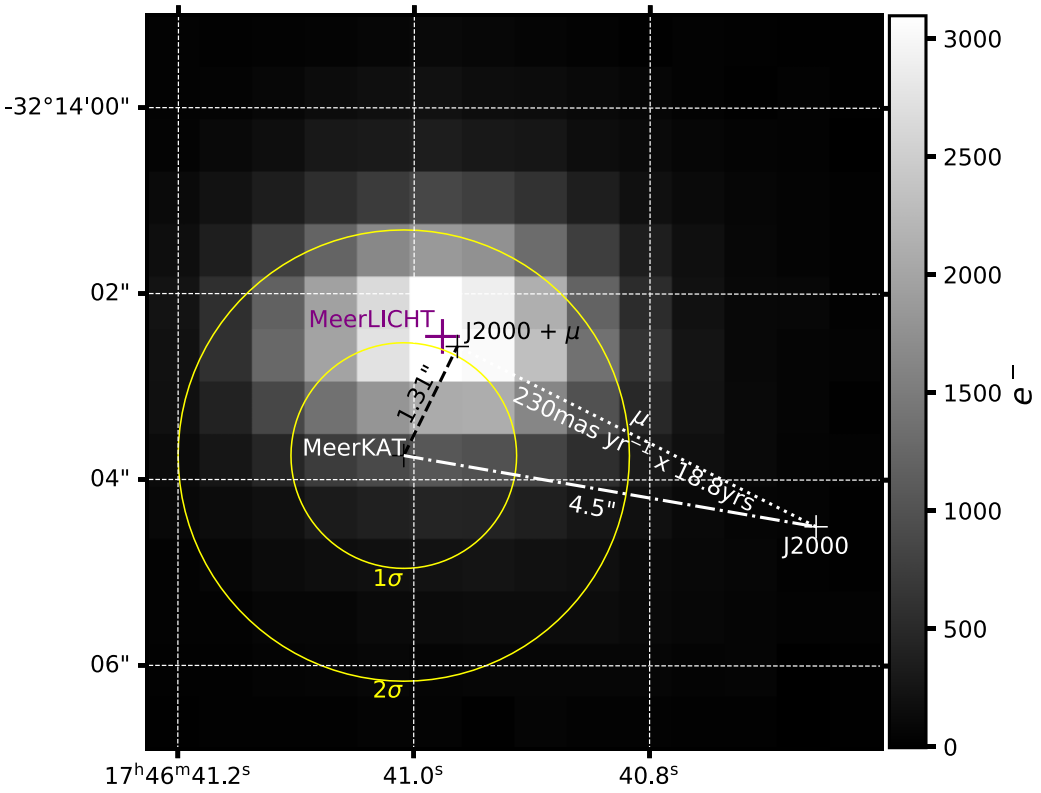

Figure 4. MeerLICHT *q*-band (440–720 nm) reference image (pixels) of the region near radio source MKT J174641.0−321404. 1σ and 2σ positional uncertainties on the MeerKAT position (circles) show an overlap between the MeerLICHT object and the *Gaia* proper motion attributed to SCR 1746.

Table 1. Select magnitudes of red dwarf SCR 1746−3214 across the visible and near-IR spectrum. Bands are listed with their effective wavelength $\lambda_{\rm eff}$.

Band ($\lambda_{\rm eff}$) (μm)	Magnitude (mag)	Uncertainty (mag)	Reference
B (0.45)	17.97	0.04	Page et al. (2012)
V (0.55)	15.6	0.2	Stassun et al. (2019)
G (0.62)	13.9734	0.0006	Gaia Collaboration et al. (2018)
I (0.88)	12.98	0.30	Sebastian et al. (2021)
J (1.25)	10.35	0.02	Cutri et al. (2003)
H (1.65)	9.74	0.03	’
K (2.16)	9.38	0.02	’
*W*1 (3.35)	9.18	0.03	Cutri et al. (2013)
*W*2 (4.6)	9.07	0.3	’
*W*3 (11.6)	8.82	0.10	’
*W*4 (22.1)	8.1	0.4	’

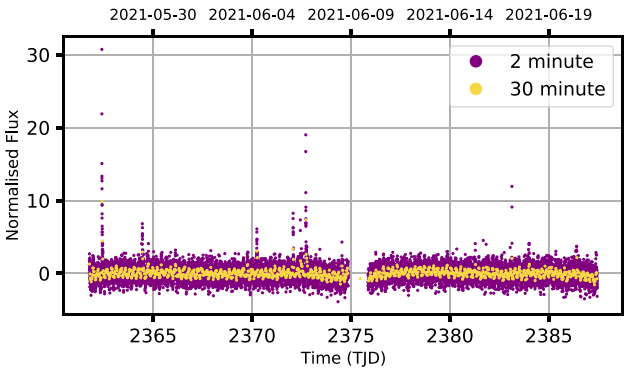

Figure 5. The *TESS* light curve of SCR 1746 (Tess Input Candidate 111898820) spanning 27.9 d from 2021 May to June, including the 2-min cadence data (purple) and the same data binned down to 30-min cadence.[3] Flare amplitudes can be seen up to 30× above non-flaring times.

the corona accelerates a population of non-thermal electrons that emit at radio frequencies via gyrosynchrotron emission. These electrons also heat the chromosphere of the star, producing thermal X-ray emission. Note that coherent emission processes are known to violate this relationship, as shown by Callingham et al. (2021), making agreement with the Güdel and Benz relation an effective diagnostic of emission mechanism (see Section 5).

Fig. 8 shows the quiescent limits and flare magnitude of SCR 1746 in comparison to other M dwarfs and other types of active star. This figure shows that M- and K-type dwarfs, some suffixed ‘e’ to denote emission lines (dM/dMe and dKe, pink triangles and yellow diamonds, respectively) tend to have lower radio and X-ray luminosities than the RS CVn binaries denoted by black circles. The quiescent radio limit for SCR 1746 is 3× the lowest rms noise floor across the individual MeerKAT epochs, measured locally using PYBDSF to be $\sim 22\,\mu$Jy. This corresponds to a specific luminosity upper limit of 1×10^{13} erg s^{-1} Hz^{-1}, an order of magnitude below the brightest observed flare at $(1.0 \pm 0.1) \times 10^{14}$ erg s^{-1} Hz^{-1}. We note that these are only approximate positions of the SCR 1746 in the figure, as the quiescent radio and X-ray emission measurements should be taken simultaneously, which has not been the case here.

Downloaded from https://academic.oup.com/mnras/article/513/3/3482/6567874 by Deutsches Elektronen Synchrotron DESY user on 05 June 2022

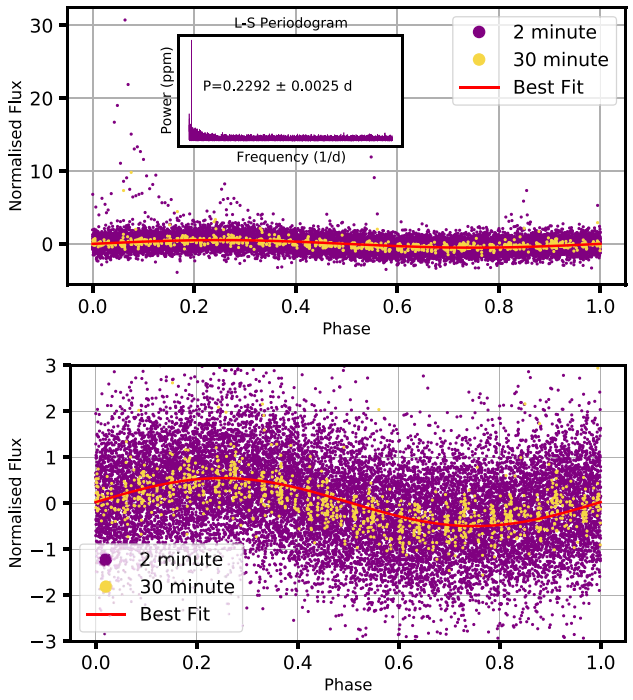

Figure 6. *Upper:* The phase folded *TESS* light curve of SCR 1746, with the corresponding Lomb–Scargle periodogram inset. Flares tend to occur between 0.0 and 0.4 in phase, corresponding to the brighter parts of the quiescent light curve. A sinusoidal best fit to the unbinned data is plotted, showing a relative amplitude of 0.52 ± 0.01. *Lower:* A closer view at the non-flare behaviour of the phase-folded light curve, in which the amplitude of the best-fitting sine curve is clearly visible. The 30-min cadence data reduce the scatter and falls in good agreement with the sinusoid.

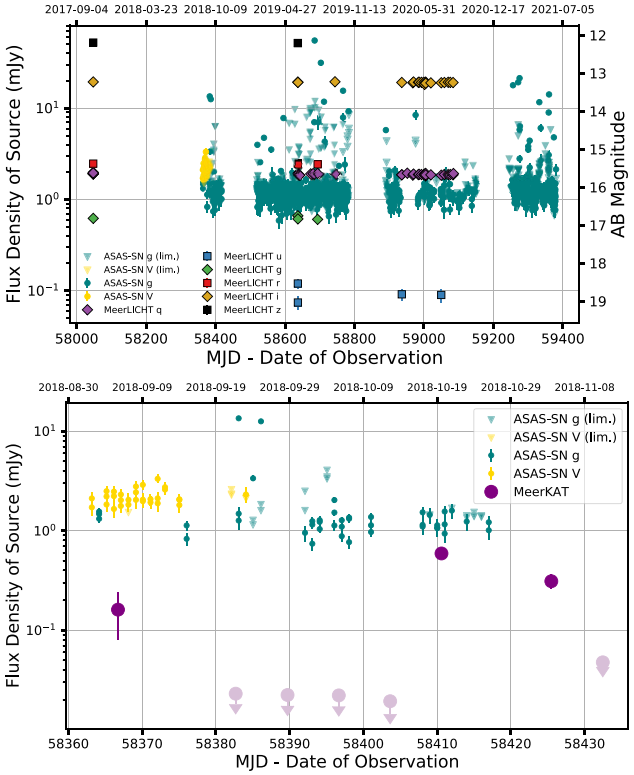

Figure 7. *Upper:* Optical data from MeerLICHT and ASAS-SN. Flaring behaviour can be seen in data from the ASAS-SN Sky Patrol portal between radio observations and mid-2021. Downwards facing triangles indicate upper limits in their respective bands. *Lower:* The radio light curve of SCR 1746 overlaid with the simultaneous optical data. No flares are simultaneous to within <0.4 d with those in the other bands.

4 OPTICAL SPECTROSCOPY

SCR 1746 was observed with the 11-m Southern African Large Telescope (SALT; Buckley, Swart & Meiring 2006) to provide confirmation of spectral type and investigate the magnetic activity of the star. Two consecutive 1000 s exposures were taken using SALT's High Resolution Spectrograph (HRS; Bramall et al. 2012; Crause et al. 2014) starting at UT 23:49:05 on the 2021 July 11th at a seeing of ∼2″.0. The HRS is a high dispersion Échelle spectrograph and was operated in low-resolution mode at a spectral resolving power of ∼16 500. Wavelength calibration is performed relative to ThAr arc spectra on a weekly basis and the data were reduced accounting for trimming, bias subtraction, gain correction, cosmic ray cleaning, and flat fielding, done via PYSALT[4] (Crawford et al. 2016). Whilst HRS is dual beam, providing both blue (370–555 nm) and red (555–890 nm) spectra, as archival photometry indicates SCR 1746 is highly red, we opt to only analyse the latter.

The two red spectra taken of SCR 1746 can be seen in Fig. 9. The extensive structure at wavelengths >7000 Å is typical for late M dwarfs and is caused by absorption due to molecules such as TiO, whilst Hα can also be seen in emission at ∼6560 Å. Following the prescription of Newton et al. (2017), the equivalent widths (EWs) of the Hα emission line integrated between 6558.8 and 6566.8 Å were calculated relative to a continuum level either side of the feature, between 6500–6550 and 6575–6625 Å. The mean EW and its standard deviation of the two spectra are −5.5 ± 0.2 Å placing

[4]http://pysalt.salt.ac.za/

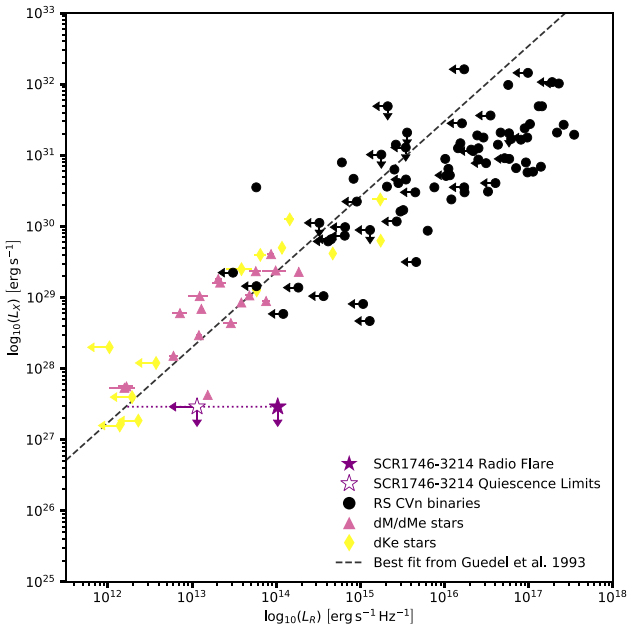

Figure 8. X-ray and radio luminosities of several types of active star (Guedel & Benz 1993) – reproduced from https://github.com/AstroLaura/GuedelPlot. Limits on SCR 1746's quiescent emission show this is an intrinsically faint source and could be approximately consistent with the Güdel and Benz relation for M dwarf (dM/dMe) stars. The radio flare is also plotted, showing a brightness increase of over an order of magnitude above quiescent limits.

Downloaded from https://academic.oup.com/mnras/article/513/3/3482/6567874 by Deutsches Elektronen Synchrotron DESY user on 05 June 2022

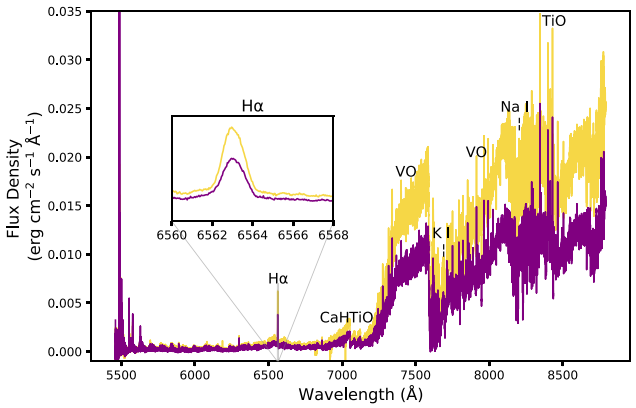

Figure 9. Two reduced spectra of SCR 1746−3214, taken by SALT. Some notable spectral features have been indicated, including clear Hα emission and molecular lines, estimated from Kirkpatrick et al. (1991). Inset is a view of the Hα emission line, which shows rotational broadening (see Section 5).

SCR 1746 clearly in the population of magnetically active stars (EW ≤ -1 Å; see Newton et al. 2017).

In order to estimate a spectroscopic classification and metallicity for SCR 1746, data were compared to co-added templates of individual stellar spectra from the Sloan Digital Sky Survey's Baryon Oscillation Spectroscopic Survey (SDSS BOSS; Dawson et al. 2013) using the spectral typing code PYHAMMER (Kesseli et al. 2017; Roulston, Green & Kesseli 2020).[5] The weighted mean and variance of 34 spectral indices from all co-added spectra across spectral types O5 through L3 and metallicities $-2.0 <$ [Fe/H] $< +1.0$ dex provide the empirical models against which chi-squared minimization is performed relative to the same features in the input spectra. The model of smallest chi-squared is therefore the closest to the input spectra and visual inspection allows for confirmation of this. Using this analysis, the best-fitting empirical template for both SALT spectra is of an M8 star with metallicty $Z = -0.5$. We can take the standard deviations of the PYHAMMER results when tested on their own SDSS BOSS spectra i.e. those used to build the empirical templates, as pessimistic estimates for uncertainties in classification and metallicity Z, which come to ± 1.5 spectral subtypes and ± 0.4 dex, respectively (see the appendix of Kesseli et al. 2017 for more on this).

5 DISCUSSION

Commensal analysis of MeerKAT images of the sky surrounding H1743−322 identified a new radio transient, MKT J174641.0−321404, coincident with the high proper motion star SCR 1746−3214. The radio flaring seen in late 2018 was detected three times over 11 epochs of data from MeerKAT. This marks the second serendipitous, Galactic transient discovered by the ThunderKAT team, both associated with kinds of active star. SCR 1746 is also the second M dwarf detected by MeerKAT (see likely quiescent emission from targeted searches of ThunderKAT commensal data in Driessen et al. 2021). Being only a few arcminutes from the black hole XRB H1743−322, more commensal observations of the flare star are likely if the XRB enters an outburst phase over the coming few years.

[5] https://github.com/BU-hammerTeam/PyHammer

The brightness temperature T_b of a source is a useful diagnostic of emission mechanism. For radio emission of flux density f_ν observed at a distance d and frequency ν

$$T_b = 2 \times 10^9 \left(\frac{f_\nu}{\mathrm{mJy}}\right) \left(\frac{\nu}{\mathrm{GHz}}\right)^{-2} \left(\frac{d}{\mathrm{pc}}\right)^2 \left(\frac{L}{R_{\mathrm{Jup}}}\right)^{-2} \mathrm{K} \quad (3)$$

(Dulk 1985; Burgasser & Putman 2005), where R_{Jup} is the radius of Jupiter. We take length-scale L to be 2 stellar radii (radius $\sim 0.146 R_\odot$ from the TIC; Stassun et al. 2019), the approximate size of M dwarf corona (Benz, Alef & Guedel 1995). For the brightest radio detection this produces a brightness temperature of $\sim 10^{10}$ K. We can relax the assumption of a length-scale by taking the variation on time-scales ~ 3 min (see the lower panel of Fig. 3) to correspond to a maximum emitting region. Doing so produces a minimum brightness temperature of 9×10^7 K. This is below the expected 10^{12} K maximum for incoherent emission and so the mechanism could be either incoherent or coherent in nature. The clearest evidence for a coherent mechanism would be the presence of high degrees of circular polarization, a measurement we do not currently have as the appropriate calibration for short-integration MeerKAT data not at phase-centre are still being developed. A factor of $\gtrsim 10$ brightness increase on quiescent emission lasting for time-scales of at least minutes is also in keeping with incoherent radio bursts (Osten 2007). Futhermore, the magnetic activity seen by the measured Hα EW and the approximate position of SCR 1746 on the Güdel and Benz relation (Fig. 8) suggest that gyrosynchrotron emission is responsible for the observed emission. Further radio observations such as polarimetry, broader frequency coverage to constrain the spectral index, or simply a longer observation campaign will help determine the exact nature and frequency of the radio flares.

Optical photometry clearly indicates SCR 1746 is bright and red, with photometric relations suggesting a mid-M spectral type. This is in mild disagreement with the findings from the SALT spectrograph when run through PYHAMMER, which indicates a later spectral type of M8 (see Section 4 and Fig. 9 therein), thus suggesting it falls under the ultracool dwarf designation. The properties of ultracool dwarfs beyond spectral type M7 depart from expectations set by earlier types (Berger 2002; Burgasser & Putman 2005; Berger et al. 2010), in the most extreme cases deviating from the Güdel and Benz relation (plotted in Fig. 8) by four orders of magnitude (e.g. Berger et al. 2001). These ultracool dwarfs show a marked decrease in magnetic activity (seen in reduced relative Hα flux) and relative X-ray flux, but an almost constant level of radio emission, i.e. the relevant coupling between wavebands appears to no longer hold in ultracool dwarfs. For example, Callingham et al. (2021) demonstrate that radio emission of 19 M dwarfs detected at 144 MHz deviate from the Güdel and Benz relation and are caused by coherent processes i.e. different to that detected for late-type stars at gigahertz frequencies and not related to their chromospheric activity. To provide a relative Hα to bolometric flux density we employ the χ method of Walkowicz, Hawley & West (2004). Calculating χ from SCR 1746's $(i - J)$ colour (Douglas et al. 2014), then $L_{\mathrm{H}\alpha}/L_{\mathrm{bol}} = \mathrm{EW}_{\mathrm{H}\alpha} \times \chi = (8.1 \pm 2.5) \times 10^{-5}$. This relatively strong Hα flux is again in agreement with a spectral type M5–M6, before the breakdown of the radio–X-ray–Hα couplings (see fig. 5 of Berger et al. 2010). Furthermore, the spectral indices of late M dwarfs are not well characterized – Kesseli et al. (2017) use seven M8 dwarfs to calculate their spectral indices, compared to a sample of 184 M5 stars – so it is perhaps not surprising that the empirical spectroscopic analysis is in disagreement with all other wave bands. As such we conclude that SCR 1746 is of spectral type at least M5 but note that a later spectral-type may be possible.

Downloaded from https://academic.oup.com/mnras/article/513/3/3482/6567874 by Deutsches Elektronen Synchrotron DESY user on 05 June 2022

The *TESS* monitoring of SCR 1746 (Figs 5 and 6) shows clear optical flares, along with a photometric modulation of relative amplitude 0.52 ± 0.01 at a period of 0.2292 ± 0.0025 d. We suggest that the photometric period observed is the rotational period of the star (as in e.g. Gizis et al. 2017) and can check this by comparing the inferred tangential velocity to that calculated by the broadening of spectral lines in the SALT data (Fig. 9, inset). For example, Lane et al. (2007) reconcile the photometric period of a radio-detected M dwarf with its spectroscopically inferred rotational velocity, invoking magnetically induced spots as the cause of periodic variability. Spectral lines are expected to be broadened due to rotation and from their width we can estimate $v\sin(i)$, not accounting for the star's inclination i with respect to our line of sight. We assume a simple relationship for rotational velocity to be $v\sin(i) = \Delta\lambda c/\lambda = \mathrm{FWHM}_{\mathrm{H}\alpha} c/2\lambda_{\mathrm{H}\alpha}$ where the factor of 2 accounts for the effect of both blueshifted and redshifted radial motion. Using the SALT data $v\sin(i) = 33.0 \pm 1.0$ km s^{-1}, in excellent agreement with the photometric inferred velocity of 32.2 ± 0.9 km s^{-1}. This therefore agrees with the idea that the modulation is rotational in nature, is consistent with previous findings that fast rotators are magnetically active (e.g. Newton et al. 2017), and even implies a high inclination of the star with respect to our line of sight. Additionally, the flares in the *TESS* data tend to occur when the source is brighter or increasing in brightness (Fig. 6), also in agreement with the light-curve modulation being caused by large magnetically active regions rotating into view.

The optical broad-band behaviour of SCR 1746 according to ASAS-SN (Fig. 7) appears to show clear and regular optical flares, which again is to be expected from a mid-late M dwarf (Paudel et al. 2018). During the times of radio observations, no flares in either waveband are simultaneous to within 0.4 d of observations in the other. This demonstrates the value of simultaneous radio–optical observations to further constrain source properties, something now provided by the MeerKAT-MeerLICHT coupling. If the black hole XRB H1743−322 enters another outburst during ThunderKAT's lifetime, then this will provide a good opportunity for multiwavelength, simultaneous follow up.

The M dwarf population in general is expected to harbour many potential exoplanets, due to the abundance of hosts (Henry 2006) and estimated occurrence rate of ∼1.2 planets per star, increasing at later spectral types (Hardegree-Ullman et al. 2019). Therefore, host star variability is a crucial consideration in understanding planet habitability. Namely, the flares produced by M dwarfs can be orders of magnitude larger than solar flares (Lacy et al. 1976) and, along with associated space weather events such as coronal mass ejections (CMEs), are likely to erode the atmospheres of planets (Lammer et al. 2007), affecting UV surface dosage, greenhouse warming efficiency and surface water retention (Airapetian et al. 2017). This is thought to most affect planets close enough to their host to sustain liquid water, as at this distance from an M dwarf they are expected to be tidally locked to their host, resulting in small magnetic moments and a weak magnetic shield to protect against CME plasma (Khodachenko et al. 2007). Flares and superflares have been recorded from known planet or planet-candidate hosting M dwarf systems (Günther et al. 2020; Lin et al. 2021) including the seven planets hosted by TRAPPIST-1, a nearby (12 pc) active M8 dwarf (Gillon et al. 2017; Luger et al. 2017). Flaring has even been seen from our planet hosting, stellar nearest-neighbour Proxima Centauri (Anglada-Escudé et al. 2016; Damasso et al. 2020), wherein ASKAP's unique capabilities provided identification of a solar type IV burst, whose occurrence is strongly associated with space weather events (Zic et al. 2020). Given the nature of the source, multiwavelength studies of SCR 1746 will be helpful in understanding the space weather around M dwarfs, determining the habitability of any potential orbiting planets.

6 CONCLUSIONS

We have reported on the serendipitous detection of MKT J174641.0−321404, a radio flaring transient source discovered in commensal searches of images from the H1743−322 radio field taken by MeerKAT. This is the second Galactic serendipitous transient found with MeerKAT, demonstrating the unique capabilities of the current generation of radio telescopes for commensal science. MKT J174641.0−321404 is coincident with M dwarf SCR 1746−3214, which, based on archival optical and X-ray photometry and dedicated SALT spectroscopy, is of mid-late M spectral type, near the transition between mid-M dwarfs and ultracool systems. *TESS* observations of SCR 1746−3214 show clear stellar flares, demonstrating it is an active star, whilst the observed periodic variability is rotational in nature and likely caused by the presence of magnetically active regions. These observations emphasize the necessity for multiwavelength association in understanding the nature of the transient sky, one of the core drivers of the MeerLICHT project.

ACKNOWLEDGEMENTS

The authors would like to thank Suzanne Aigrain, Baptiste Klein, and Sophia Vaughan for their helpful discussions. AA, LR, and NE acknowledge the support given by the Science and Technology Facilities Council through STFC studentships. CJL acknowledges support from the Alfred P. Sloan foundation. LND acknowledges support from the European Research Council (ERC) under the European Union's Horizon 2020 research and innovation programme (grant agreement No. 694745). DAHB acknowledges reseach support from the National Research Foundation. PJG acknowledges support from NRF SARChI Grant 111692. MeerKAT is operated by the South African Radio Astronomy Observatory (SARAO), which is a facility of the National Research Foundation, an agency of the Department of Science and Innovation. The MeerLICHT consortium is a partnership between Radboud University, the University of Cape Town, the Netherlands Organisation for Scientific Research (NWO), the South African Astronomical Observatory (SAAO), the University of Oxford, the University of Manchester and the University of Amsterdam, in association with and, partly supported by, the South African Radio Astronomy Observatory (SARAO), the European Research Council and the Netherlands Research School for Astronomy (NOVA).

We thank the SARAO and SAAO staff involved in obtaining the MeerKAT and SALT observations. The SALT observations were obtained under the SALT transient followup programme 2018-2-LSP-001 (PI: DAHB). We acknowledge the use of the Inter-University Institute for Data Intensive Astronomy (IDIA) data intensive research cloud for data processing. IDIA is a South African university partnership involving the University of Cape Town, the University of Pretoria and the University of the Western Cape.

This research has made use of the SIMBAD data base, operated at CDS, Strasbourg, France (Wenger et al. 2000). This work has made use of data from the European Space Agency (ESA) mission *Gaia* (https://www.cosmos.esa.int/gaia), processed by the *Gaia* Data Processing and Analysis Consortium (DPAC, https://www.cosmos.esa.int/web/gaia/dpac/consortium). Funding for the DPAC has been provided by national institutions, in particular the institutions

Downloaded from https://academic.oup.com/mnras/article/513/3/3482/6567874 by Deutsches Elektronen Synchrotron DESY user on 05 June 2022

participating in the *Gaia* Multilateral Agreement (Gaia Collaboration 2016, 2018; Bailer-Jones et al. 2018).

This research has made use of ASTROPY, an Astronomy-based, community-developed PYTHON package (Astropy Collaboration 2013, 2018).

DATA AVAILABILITY

All data required to reproduce results, figures, and calculations herein can be found at the relevant GitHub repository: https://github.com/AnderssonAstro/MKT-J174641.0-321404-Paper-Figures Please cite the following Digital Object Identifier if any of the code and data are useful to your research: https://doi.org/10.5281/zenodo.6346829

REFERENCES

Airapetian V. S.,Glocer A., Khazanov G. V., Loyd R. O. P., France K., Sojka J., Danchi W. C., Liemohn M. W., 2017, ApJ, 836, L3
Anglada-Escudé G. et al., 2016, Nature, 536, 437
Astropy Collaboration, 2013, A&A, 558, A33
Astropy Collaboration, 2018, AJ, 156, 123
Bailer-Jones C. A. L., Rybizki J., Fouesneau M., Mantelet G., Andrae R., 2018, AJ, 156, 58
Bannister K. W.,Murphy T., Gaensler B. M., Hunstead R. W., Chatterjee S., 2011, MNRAS, 412, 634
Bastian T. S., 1990, Solar Physics, 130, 265
Benz A., Guedel M., 1994, A&A, 285, 621
Benz A., Alef W., Guedel M., 1995, A&A, 298, 187
Berger E., 2002, ApJ, 572, 503
Berger E. et al., 2001, Nature, 410, 338
Berger E. et al., 2010, ApJ, 709, 332
Bhandari S. et al., 2018, MNRAS, 478, 1784
Bloemen S. et al., 2016, in Hall H. J., Gilmozzi R., Marshall H. K., eds, Proc. SPIE Conf. Ser. Vol. 9906, Ground-based and Airborne Telescopes VI. SPIE, Bellingham, p. 990664
Bower G. C., Saul D., Bloom J. S., Bolatto A., Filippenko A. V., Foley R. J., Perley D., 2007, ApJ, 666, 346
Boyd M. R., Winters J. G., Henry T. J., Jao W. C., Finch C. T., Subasavage J. P., Hambly N. C., 2011, AJ, 142, 10
Bramall D. G. et al., 2012, in McLean I. S., Ramsay S. K., Takami H., eds, Proc. SPIE Conf. Ser. Vol. 8446, Ground-based and Airborne Instrumentation for Astronomy IV. SPIE, Bellingham, p. 84460A
Buckley D. A. H., Swart G. P., Meiring J. G., 2006, in Stepp L. M., ed., Proc. SPIE Conf. Ser. Vol. 6267, Ground-based and Airborne Telescopes. SPIE, Bellingham, p. 62670Z
Burgasser A. J., Putman M. E., 2005, ApJ, 626, 486
Callingham J. R. et al., 2021, Nat. Astron., 5, 1233
Camilo F. et al., 2018, ApJ, 856, 180
Cram L. E., Giampapa M. S., 1987, ApJ, 323, 316
Cram L. E., Mullan D. J., 1979, ApJ, 234, 579
Crause L. A. et al., 2014, in Ramsay S. K., McLean I. S., Takami H., eds, Proc. SPIE Conf. Ser. Vol. 9147, Ground-based and Airborne Instrumentation for Astronomy V. SPIE, Bellingham, p. 91476T
Crawford S. M. et al., 2016, in Evans C. J. , Simard L., Takami H., eds, Proc. SPIE Conf. Ser. Vol. 9908, Ground-based and Airborne Instrumentation for Astronomy VI. SPIE, Bellingham, p. 99082L
Cutri R. M. et al., 2003, The IRSA 2MASS All-Sky Point Source Catalog, NASA/IPAC Infrared Science Archive, Available at:http://irsa.ipac.caltech.edu/applications/Gator
Cutri R. M. et al., 2013, Explanatory Supplement to the AllWISE Data Release Products,
D'Elia V. et al., 2013, A&A, 551, 142
Damasso M. et al., 2020, Sci. Adv., 6, eaax7467
Dawson K. S. et al., 2013, AJ, 145, 10
Douglas S. T. et al., 2014, ApJ, 795, 161
Driessen L. N. et al., 2020, MNRAS, 491, 560
Driessen L. N., Williams D. R. A., McDonald I., Stappers B. W., Buckley D. A. H., Fender R. P., Woudt P. A., 2021, MNRAS, 510, 1083
Driessen L. N. et al., 2022, MNRAS, 512, 5037
Dulk G. A., 1985, ARA&A, 23, 169
Evans P. A. et al., 2014, ApJS, 210, 8
Evans P. A. et al., 2020, ApJS, 247, 54
Fender R. P., Bell M. E., 2011, Bull. Astron. Soc. India, 39, 315
Fender R. et al., 2016, Proc. Sci., ThunderKAT: The MeerKAT Large Survey Project for Image-Plane Radio Transients. SISSA, Trieste, PoS#13
Filippazzo J. C., Rice E. L., Faherty J., Cruz K. L., Van Gordon M. M., Looper D. L., 2015, ApJ, 810, 158
Gaia Collaboration, 2016, A&A, 595, A1
Gaia Collaboration, 2018, A&A, 616, A1
Gillon M. et al., 2017, Nature, 542, 456
Gizis J. E., Paudel R. R., Mullan D., Schmidt S. J., Burgasser A. J., Williams P. K. G., 2017, ApJ, 845, 33
Güdel M., 2002, ARA&A, 40, 217
Guedel M., Benz A. O., 1993, ApJ, 405, L63
Günther M. N. et al., 2020, AJ, 159, 60
Hardegree-Ullman K. K., Cushing M. C., Muirhead P. S., Christiansen J. L., 2019, AJ, 158, 75
Henry T. J., 2006, in Hartkopf W. I., Guinan E. F., Harmanec P., eds, Proc. IAU Symp. 240, Binary Stars as Critical Tools & Tests in Contemporary Astrophysics. Kluwer, Dordrecht, p. 299
Hyman S. D., Lazio T. J. W., Kassim N. E., Ray P. S., Markwardt C. B., Yusef-Zadeh F., 2005, Nature, 434, 50
Jaeger T. R., Hyman S. D., Kassim N. E., Lazio T. J., 2012, AJ, 143, 96
Jenkins J. M. et al., 2016, in Chiozzi G., Guzman J. C., eds, Proc. SPIE Conf. Ser. Vol. 9913, Software and Cyberinfrastructure for Astronomy IV. SPIE, Bellingham, p. 99133E
Johnston S. et al., 2007, Publ. Astron. Soc. Aust., 24, 174
Kesseli A. Y., West A. A., Veyette M., Harrison B., Feldman D., Bochanski J. J., 2017, ApJS, 230, 16
Khodachenko M. L. et al., 2007, Astrobiology, 7, 167
Kirkpatrick J. D., Henry T. J., McCarthy D. W. Jr, 1991, ApJS, 77, 417
Kochanek C. S. et al., 2017, PASP, 129, 104502
Lacy C. H., Moffett T. J., Evans D. S., 1976, ApJS, 30, 85
Lacy M. et al. 2020, PASP, 132, 035001
Lammer H. et al., 2007, Astrobiology, 7, 185
Lane C. et al., 2007, ApJ, 668, L163
Levinson A., Ofek E. O., Waxman E., Gal-Yam A., 2002, ApJ, 576, 923
Lin C.-L. et al., 2021, AJ, 162, 11
Lomb N. R., 1976, Ap&SS, 39, 447
Lovell B., 1969, Nature, 222, 1126
Lovell B., Whipple F. L., Solomon L. H., 1963, Nature, 198, 228
Luger R. et al., 2017, Nat. Astron., 1, 0129
McMullin J. P., Waters B., Schiebel D., Young W., Golap K., 2007, in Shaw R. A., Hill F., Bell D. J., eds, ASP Conf. Ser. Vol. 376, Astronomical Data Analysis Software and Systems XVI. Astron.Soc. Pac., San Francisco, p. 127
Mohan N., Rafferty D., 2015, Astrophysics Source Code Library, record ascl:1502.007
Monet D. G. et al., 2003, AJ, 125, 984
Mooley K. P. et al., 2016, ApJ, 818, 105
Murphy T. et al., 2013, PASA, 30, e006
Murphy T. et al., 2017, MNRAS, 466, 1944
Newton E. R., Irwin J., Charbonneau D., Berlind P., Calkins M. L., Mink J., 2017, ApJ, 834, 85
Ofek E. O., Frail D. A., Breslauer B., Kulkarni S. R., Chandra P., Gal-Yam A., Kasliwal M. M., Gehrels N., 2011, ApJ, 740, 65
Offringa A. R., Smirnov O., 2017, MNRAS, 471, 301
Offringa A. R., Van De Gronde J. J., Roerdink J. B., 2012, A&A, 539, A95
Offringa A. R. et al., 2014, MNRAS, 444, 606
Osten R. A., 2007, Proc. Sci, Bursts, Pulses and Flickering: Wide Field Monitoring of the Dynamic Radio Sky, 5
Page M. J. et al., 2012, MNRAS, 426, 903
Paudel R. R., Gizis J. E., Mullan D. J., Schmidt S. J., Burgasser A. J., Williams P. K. G., Berger E., 2018, ApJ, 858, 55

Downloaded from https://academic.oup.com/mnras/article/513/3/3482/6567874 by Deutsches Elektronen Synchrotron DESY user on 05 June 2022

Pietka M., Fender R. P., Keane E. F., 2015, MNRAS, 446, 3687
Prasad P. et al., 2016, J. Astron. Instrum., 5, 1641008
Pritchard J. et al., 2021, MNRAS, 502, 5438
Radcliffe J. F., Beswick R. J., Thomson A. P., Garrett M. A., Barthel P. D., Muxlow T. W., 2019, MNRAS, 490, 4024
Rajpurohit A. S., Reylé C., Allard F., Homeier D., Schultheis M., Bessell M. S., Robin A. C., 2013, A&A, 556, A15
Ricker G. R. et al., 2015, J. Astron. Telesc. Instrum. Syst., 1, 014003
Roulston B. R., Green P. J., Kesseli A. Y., 2020, ApJS, 249, 34
Rowlinson A. et al., 2019, Astron. Comput., 27, 111
Sarbadhicary S. K. et al., 2021, ApJ, 923, 31
Scargle J. D., 1982, ApJ, 263, 835
Sebastian D. et al., 2021, A&A, 645, 100
Shappee B. J. et al., 2014, ApJ, 788, 48
Skrutskie M. F. et al., 2006, AJ, 131, 1163
Slee O. B., Willes A. J., Robinson R. D., 2003, Publ. Astron. Soc. Aust., 20, 257
Spitzer Science Center, 2009, VizieR Online Data Catalog, II/293
Stassun K. G. et al., 2019, AJ, 158, 138
Stewart A. J. et al., 2016, MNRAS, 456, 2321
Swinbank J. D. et al., 2015, Astron. Comput., 11, 25
Tingay S. J. et al., 2012, Proc. Sci., Realisation of a low frequency SKA Precursor: The Murchison Widefield Array. SISSA, Trieste, p. PoS#36
Van Haarlem M. P. et al., 2013, A&A, 556, A2
Varghese S. S., Obenberger K. S., Dowell J., Taylor G. B., 2019, ApJ, 874, 151
Villadsen J., Hallinan G., 2019, ApJ, 871, 214
Walkowicz L. M., Hawley S. L., West A. A., 2004, PASP, 116, 1105
Wang Z. et al., 2021, ApJ, 920, 45
Wenger M. et al., 2000, A&AS, 143, 9
West A. A., Walkowicz L. M., Hawley S. L., 2005, PASP, 117, 706
Williams D. R. et al., 2020, MNRAS, 491, L29
Zic A. et al., 2019, MNRAS, 488, 559
Zic A. et al., 2020, ApJ, 905, 23

This paper has been typeset from a TEX/LATEX file prepared by the author.

Downloaded from https://academic.oup.com/mnras/article/513/3/3482/6567874 by Deutsches Elektronen Synchrotron DESY user on 05 June 2022